Article

Investigation on the Melting Performance of a Phase Change Material Based on a Shell-and-Tube Thermal Energy Storage Unit with a Rectangular Fin Configuration

Meng Yu [1,2,*], Xiaowei Sun [1], Wenjuan Su [1], Defeng Li [1], Jun Shen [1], Xuejun Zhang [2] and Long Jiang [2]

[1]   Special Equipment Safety Supervision Inspection Institute of Jiangsu Province, Nanjing 210036, China
[2]   Institute of Refrigeration and Cryogenics, Zhejiang University, Hangzhou 310027, China
*   Correspondence: ym1993@zju.edu.cn

Abstract: A case study on the melting performance of a shell-and-tube phase change material (PCM) thermal energy storage unit with a novel rectangular fin configuration is conducted in this paper. Paraffin wax and circulated water are employed as the PCM and heat transfer fluid (HTF), respectively. It can be observed that the melting performance could be significantly improved by using rectangular fins. Melting photographs demonstrate that the melting of the PCM is firstly dominated by heat conduction; then, the melting rate is improved further due to natural convection. Moreover, the results illustrate that the influence of the inlet HTF temperature on the melting performance is significantly greater than that of the inlet HTF flow rate. The liquid fraction of paraffin wax in the PCM unit with a higher inlet HTF temperature is always higher than that with a lower inlet HTF temperature at the same time. The total charging time is reduced by 62.38% and the average charging rate is increased by 165.51% when the inlet HTF temperature is increased from 57 °C to 68 °C. As a result, a higher value of the inlet HTF temperature and a lower value of the HTF flow rate are able to improve the energy efficiency of the PCM unit with a rectangular fin configuration.

Keywords: phase change material; shell-and-tube thermal energy storage unit; rectangular fin configuration; melting performance

1. Introduction

The energy crisis is a crucial issue which involves the economy, environment and society. The development of technology in energy fields for the purpose of energy saving and environmental protection has become significant [1]. In particular, renewable energy plays a more considerable role. However, the mismatch between energy demand and supply is the major defect that restricts the application of renewable energy. As a result, thermal energy storage (TES) could overcome this drawback [2]. The applications of TES are extremely extensive, including domestic hot water supply and space heating [3], refrigeration and air conditioning [4], seawater desalination [5], new energy vehicles [6], thermal power generation [7], etc.

Based on their different working principles, TES can be divided into three catalogs: sensible thermal energy storage, latent thermal energy storage and chemical thermal energy storage. With respect to sensible thermal energy storage, heat is stored through temperature differences in the materials. With respect to latent thermal energy storage (LTES), thermal energy is stored relying on the melting process of a phase change material (PCM). For chemical thermal energy storage, heat is stored in the forms of chemical potentials of working pairs. Generally, LTES has the advantages of high thermal energy storage performance and stable temperature during the charging/discharging processes compared with sensible thermal energy storage. In addition, the PCM used in LTES is more mature and reliable than that used in chemical thermal energy storage. Thus, LTES is currently the most investigated TES research field.

The shell-and-tube thermal energy storage unit is the most commonly used structure in LTES. This structure includes a heat storage container and bunches of tubes. PCM is filled into a heat storage container and HTF is pumped through the tubes, resulting in the heat transfer process between them. Many researchers have investigated system characteristics of shell-and-tube thermal energy storage units [8–10]. Most of the literature is mainly concentrated on the analysis of TES performance under different operating and geometric parameters [11–13]. Rual et al. [9] experimentally analyzed the characteristics of a vertical multi-tube shell-and-tube-based LTES system during the discharging process for solar energy utilization. The results showed that the efficiency of the heat released was increased when the HTF flow rate and initial phase change temperature were increased, and the inlet HTF temperature was decreased. Seddegh et al. [10] studied the influence of operating and geometric parameters on a shell-and-tube LTES system. The results indicated that both the shell-to-tube radius ratio and the inlet HTF temperature played important roles in the charging/discharging processes. Fornarelli et al. [11] carried out a test on a shell-and-tube LTES unit by means of a simulation coupled with heat transfer modelling including the external dissipation phenomenon. Results showed that a convective contribution to the heat transfer existed during the charging process, however, it seemed to be limited by the geometrical characteristics of the LTES unit. Kibria et al. [12] numerically and experimentally investigated charging/discharging processes in a shell-and-tube PCM unit. The results revealed that the inlet HTF temperature had a significant impact, and the tube radius was a crucial geometric parameter which was related to the performance of the unit. Seddegh et al. [13] conducted an experimental and numerical investigation on the thermal behavior and physics of heat transfer in a vertical cylindrical shell-and-tube LTES unit during both charging/discharging processes. Results indicated that liquid PCM ascended to the upper part of the unit and the melting front moved downward during the charging process, and the solidification front moved along both radial and axial directions during the discharging process. Akgun et al. [14] experimentally studied the charging/discharging processes of a shell-and-tube PCM unit. The results revealed that higher values of the inlet HTF temperature were suggested for a higher energy efficiency, while lower values of the HTF flow rate were recommended for lower energy consumptions. Medrano et al. [15] investigated charging/discharging processes of five PCM units with different structural arrangements. Results concluded that the compact heat exchanger exhibited the potential for a higher average charging rate and more heat transfer surface area during charging/discharging processes. MacPhee and Erguvan [16] numerically investigated the thermal energy performance of a shell-and-tube heat exchanger using the LTES method. Results indicated that the effect of the volume ratio on the energy efficiency was higher than that of the inlet HTF temperature, and the total charging time decreased with the decreasing volume ratio due to higher heat transfer surfaces.

However, LTES application has been significantly restricted due to its poor thermal conductivity of PCM, especially for paraffin wax. The melting/solidification process of PCM is retarded, which has an influence on the heat transfer rate and TES efficiency eventually. In this instance, several heat transfer enhancements have been developed, such as employing fins [17], employing metal foams [18], embedding heat pipes [19], dispersing high-conductivity nanoparticles [20], etc. Among all of these, employing fins by using material with high conductivity, such as aluminum, can remarkably increase the heat transfer area between the PCM and the HTF, which improves the heat transfer rate. Furthermore, the employed fins are easy to fabricate as an enhanced heat transfer structure. Several researchers have analyzed the impact of employing fins on a LTES system numerically and experimentally [21–23]. Results demonstrated that a higher heat transfer rate and faster charging/discharging processes were observed in finned LTES systems when compared to those without fins. Moreover, the optimization of fin parameters, e.g., number of fins, material of fins, fin thickness and fin pitch, has been investigated extensively to improve the internal heat transfer rate. Yang et al. [17] numerically studied the characteristics of a shell-and-tube PCM energy storage unit with annular fins during the

charging process. Results demonstrated that employing annular fins into the PCM could accelerate the heat transfer rate of the PCM, and the total charging time was able to be reduced by up to 65%. Deng et al. [24] established a numerical mathematical model based on natural convection in liquid PCM to find the most efficient fin configuration to improve the melting performance. In addition, the influences of fin number, fin length, inlet HTF temperature and tube material on the melting performance of the PCM unit were studied, and the optimal configuration of employed fins was suggested. Vogel and Johnson [25] also developed a numerical mathematical model to analyze the influence of natural convection on a shell-and-tube PCM unit with irregularly extended fins. The results showed that natural convection became more significant when the tube spacing became larger and fin fraction become lower. Deng et al. [26] developed a numerical simulation to analyze the melting performance of a LTES unit with fins. In particular, the fins were employed in the lower part of the PCM unit along with a copper tube symmetrically. The results indicated that the influence of shell conductivity played an important role in the melting performance. It was also found out that the melting performance could be enhanced by using longer fins. Bhagat et al. [27] numerically developed a model by using the enthalpy method to present melting/solidification processes of PCM in a fin-and-tube unit. Results revealed that geometric parameters of fins, especially the number of fins and fin thickness, were more important for the characteristics of the LTES unit compared with the thermal conductivity of the fin material.

Based on the summarization of the above research, it is worth noting that the configurations of annular fins [17] or longitudinal fins [22] are the main research objectives of LTES. To the best of the authors' knowledge, experimental or visualized research on the melting performance of PCM has been rarely reported in terms of the influence of HTF operating parameters. A further investigation for a rectangular fin configuration in a shell-and-tube unit has been conducted.

In this paper, the influence of HTF operating parameters during the charging process on a shell-and-tube unit was experimentally investigated based on a novel rectangular fin configuration. An experimental setup was established for case studies. The rectangular fins were placed equidistantly along the axial direction of the copper tube in the LTES unit. Different inlet HTF temperatures and flow rates were considered and compared. The optimal HTF parameters were determined for maximizing the characteristics of the LTES unit. This work could provide considerable guidance and experience to relevant researchers for designing shell-and-tube LTES units with rectangular fins.

2. Materials and Methods

2.1. Materials

Paraffin wax was selected as the PCM used in the LTES unit due to its stable thermophysical properties. Furthermore, the specific phase change temperature of paraffin wax is suitable for TES of domestic hot water and space heating. Table 1 presents the thermophysical properties of the paraffin wax used in this study [28]. In addition, a sample of the paraffin wax was also analyzed using a differential scanning calorimeter (DSC) device, as shown in Section 3.1.

Table 1. Thermophysical properties of paraffin wax used.

Property	Value	Unit
Phase change temperature	48–50	[°C]
Specific heat capacity	2.6	[kJ/(kg·K)]
Phase change latent heat	210	[kJ/kg]
Density in solid (at 20 °C)	0.88	[kg/L]
Density in liquid (at 80 °C)	0.77	[kg/L]
Thermal conductivity	0.2	[W/(m·K)]
Volume expansion	12.5	[%]
Thermal expansion coefficient	5.9×10^{-4}	[1/K]

2.2. Experimental Setup

Figure 1 shows a system schematic diagram of the experimental setup. The components in the experimental setup included a hot water tank, a cut-off valve, a circulating pump, a PCM unit, a flow meter and several sections of pipelines. Circulated water was selected as the HTF to evaluate its influence on the melting performance of the PCM.
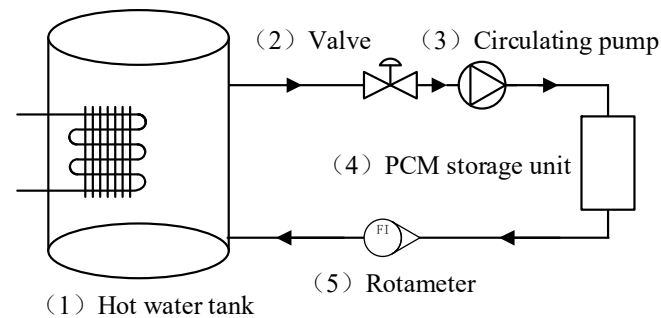

Figure 1. A system schematic diagram of the experimental setup.

Figure 2 depicts a configuration of the specific PCM unit utilized. The geometric structure of the PCM unit was considered as a rectangular shell-and-tube thermal accumulator with a single tube and rectangular fins. The PCM was kept in the rectangular space between the finned tube and the shell. In addition, the finned tube and shell were concentrically placed. The tube was composed of copper and the fins were composed of aluminum due to the excellent thermal conductivity. The outer shell was composed of organic glass for better visualization of the melting performance. The rectangular space was filled with paraffin wax and the HTF flowed through the finned tube from right to left. Table 2 shows the geometric parameters of the PCM unit.
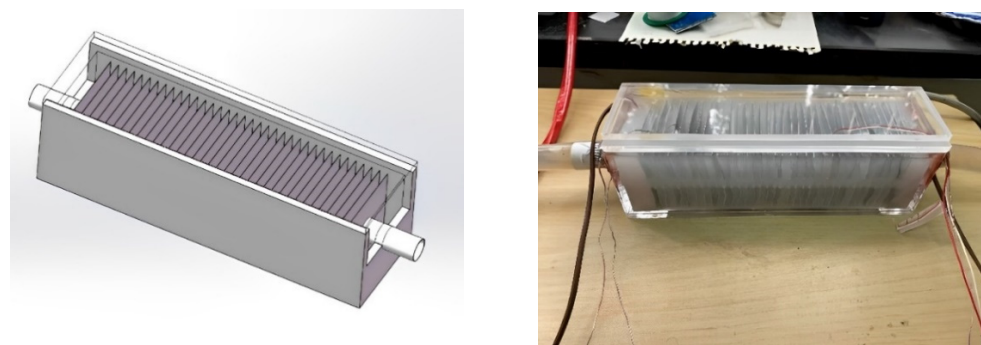

Figure 2. Configuration of specific PCM unit.

Table 2. Geometric parameters of the PCM unit.

Parameter	Value	Unit
Shell width	64	[mm]
Shell depth	64	[mm]
Shell length	210	[mm]
Shell thickness	5	[mm]
Tube length	250	[mm]
Inner diameter of tube	13.8	[mm]
Tube thickness	0.7	[mm]
Dimensions of fins	50×50	[mm]
Fin thickness	0.15	[mm]
Fin pitch	5	[mm]
Number of fins	36	[-]
PCM volume	0.55	[L]

Figure 3 shows the specific locations of the thermocouples arranged in the PCM unit. Six thermocouples were utilized to monitor the temperature field in the unit, including the PCM temperature between the fins (T_{103}), fin temperatures (T_{102} and T_{104}), PCM temperature without fins (T_{105}), inlet HTF temperature (T_{101}) and outlet HTF temperature (T_{106}). All thermocouples were calibrated in advance by means of comparison between standard and calibrated thermocouples using a temperature calibration furnace, and the measuring range and accuracy of these thermocouples were −20~100 °C and ±0.2 °C, respectively. The temperature calibration furnace used in this study was a high-precision, multi-functional temperature-measuring testing product, and its machine type and temperature range were SPMK313A and −33~155 °C, respectively. The calibration method could be listed as follows: (1) The tested thermocouples were evenly surrounded around the standard thermocouple and tied up together when their measuring ends were on the same vertical plane. (2) The thermocouples were placed in the temperature calibration furnace, a specific temperature value was set and the thermoelectric potentials of the tested and standard thermocouples were measured, respectively. (3) The deviations between the tested thermocouples and the indexing table at the specific temperature points were calculated using the thermoelectric potentials on the indexing table, the potential values of the specific temperature points in standard certification and the differential thermoelectric potentials at each scale point of the thermocouples. In addition, a data acquisition module was used to collect and record the measuring temperatures once every 3 s during the charging process.
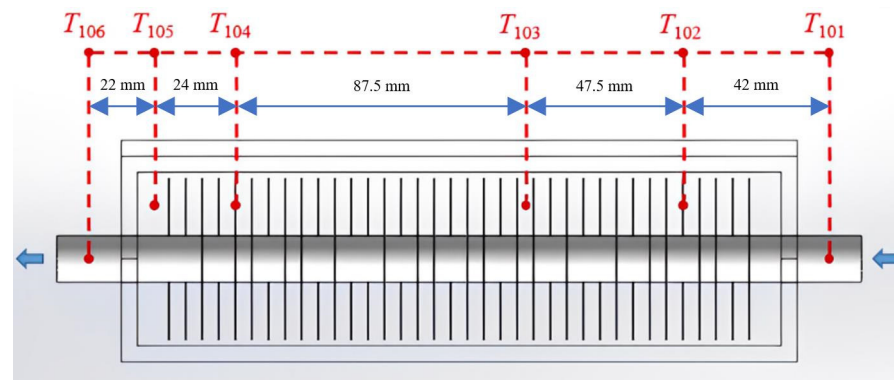

Figure 3. Specific locations of thermocouples arranged in the PCM unit.

To provide accurate and stable HTF parameters in the experimental setup, the hot water tank used in the experiment was equipped with an adjustable thermostat under a sensitivity of ±0.2 °C. A variable speed pump was applied to circulate the HTF through the PCM unit. A rotameter with a maximum capacity of 18 L/min and accuracy of ±2% was employed to measure the HTF flow rate in the experiment. For more information, please refer to Table 3.

Table 3. List of measuring instruments used in the test platform.

Component	Type	Parameter
Circulating pump	MP-20R	Voltage: 220 V; nominal power: 15 W; nominal capacity: 27 L/min; nominal lift: 3.1 m
Rotameter	Liquid-LZM-15	Measuring range: 2~18 L/min; accuracy: ±2%
Thermocouples	T type	Measuring range: −20~100 °C; accuracy: ±0.2 °C

2.3. Experimental Procedure

The paraffin wax used in the PCM unit was initially in the form of white slices. The sliced paraffin wax was heated up to 80 °C in the oven before filling the unit. After that, the melted paraffin wax was poured into the unit gradually in layers, and the height of each layer was no more than 10 mm. Moreover, the new layer was not added until the previous layer was completely solidified. Finally, the whole PCM unit was filled with solid

paraffin wax. The purpose of this filling procedure was to guarantee that no bubbles were formed inside the solid paraffin wax. Meanwhile, the thermocouples which measured the fin, inlet and outlet HTF temperatures were directly fixed on the measuring locations with the help of tinfoil before filling the PCM unit with the paraffin wax. The thermocouples which measured the PCM temperatures between fins and without fins were fixed on the measuring locations at certain depths during the filling of the PCM unit with the paraffin wax. After the solidification of the liquid PCM, the outer parts of the thermocouples were fixed on the PCM unit with tinfoil in order to prevent the measuring locations from shifting during the melting process.

The charging process started when hot HTF passed through the PCM unit. In order to make a comparison, the initial PCM temperature was kept constant at approximately 25 °C. The inlet HTF temperature was controlled using the hot water tank in the experimental setup, and the HTF flow rate was controlled using the opening degree of the valve. It should be noted that the leakage of liquid paraffin wax appeared for the first melting performance test due to the different densities of the solid and liquid paraffin wax, since the PCM unit was full of solid paraffin wax during the filling procedure. Therefore, it was necessary to remove the liquid paraffin wax from the upper part of the PCM unit during the first melting process. After the first melting performance test was completed and the paraffin wax was solidified, it was found that a small groove was formed from the solid paraffin wax in the upper part of the PCM unit. After this, no further leakage of liquid paraffin wax happened again. The melting process was supposed to end as the temperature in the PCM region approached a relatively stable value which was slightly higher than the melting temperature of the paraffin wax. All case studies were carried out three times to guarantee the accuracy of the results.

2.4. TES Characteristics Indexes

The melting performance of the PCM unit was quantitatively evaluated using TES characteristics indexes, such as the total charging time (t_{ch}) and the average charging rate (P_{ch}) [29]. The total charging time was obtained by monitoring the PCM temperature and its changing rate, while the average charging rate was determined using the following equations.

$$Q_{ch} = \sum_{i=0}^{n-1} c_p q_{HTF}(T_{in} - T_{out})(t_{i+1} - t_i) \tag{1}$$

$$P_{ch} = \frac{Q_{ch}}{t_{ch}} \tag{2}$$

where Q_{ch} represented the total TES of the PCM unit during the charging process (J), c_p was the HTF specific heat capacity (J/(kg·K)), q_{HTF} was the HTF flow rate (kg/s), T_{in} and T_{out} were the inlet and outlet HTF temperatures (°C), respectively, and n was the number of time intervals.

2.5. Uncertainty Analysis

An uncertainty analysis was conducted based on the method given in [30]. The uncertainty of the final results was determined using the root mean square of the measured variables. The uncertainty of the experimental results was estimated using the following equations.

$$f = (T, q, m, l) \tag{3}$$

$$\frac{\Delta f}{f} = \sqrt{\left(\frac{\Delta T}{T}\right)^2 + \left(\frac{\Delta q}{q}\right)^2 + \left(\frac{\Delta m}{m}\right)^2 + \left(\frac{\Delta l}{l}\right)^2} \tag{4}$$

The thermocouples had a measuring range of −20~100 °C and an accuracy of ±0.2 °C, respectively. The uncertainties of the HTF flow rate, paraffin wax mass and locations of thermocouples were ±2% of the maximum flow rate (18 L/min), ±1 g of the total paraffin wax mass (0.39 kg) and ±0.02 mm of the PCM unit (50 mm), respectively. Thus, the

final uncertainty of experimental results was eventually calculated to be ±2.02% using Equation (4).

3. Results

3.1. Material Analysis

　　The DSC thermal analysis was performed under the heating rate of 5 °C/min. Figure 4 illustrates the DSC curves of the paraffin wax which was used. The positive heat flow indicates the heat absorbed by the paraffin wax during the melting process (Figure 4a), and the negative heat flow indicates the heat released by the paraffin wax during the solidification process (Figure 4b). Two peaks were observed in the melting and solidification processes. For the melting process, the first peak at approximately 37 °C corresponds to the solid–solid phase transition procedure between the two paraffin structures formed, while the second peak at approximately 55 °C corresponds to the solid–liquid phase change procedure of the paraffin wax. The second peak was caused by the combination of sensible and phase change thermal energy storage.
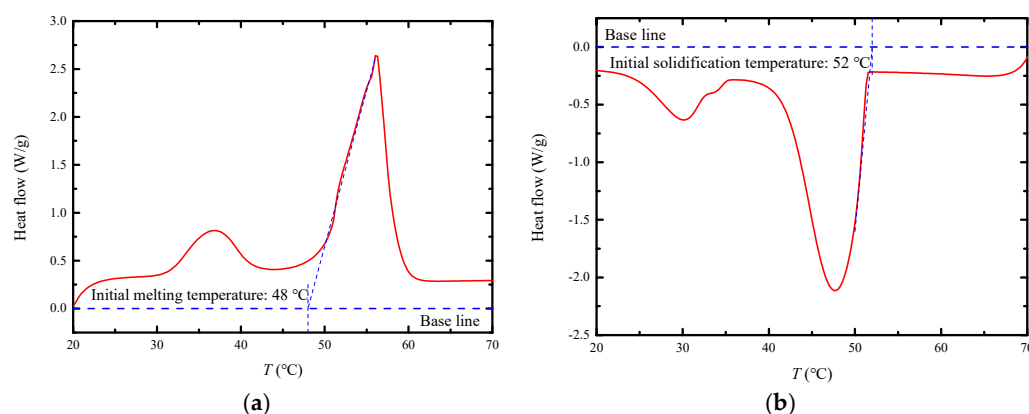

Figure 4. DSC results of the paraffin wax. (**a**) Melting; (**b**) solidification.

　　The melting/solidification temperature (T_m/T_s) and phase change latent heat (ΔH_m) of the paraffin wax were determined based on a DSC thermal analysis, as listed in Table 4. The melting temperature represents the initial phase change temperature of the paraffin wax during the charging process, and the solidification temperature represents the initial phase change temperature of the paraffin wax during the discharging process. The latent heat of the paraffin wax was obtained with the numerical integration of the area under the second peak in Figure 4a. However, the latent heat value obtained with the DSC thermal analysis was a little different from that provided in Table 1. The different methods used to determine the specific value of latent heat of paraffin wax may have caused this to happen. Therefore, the thermophysical properties of paraffin wax used in the following analysis were subjected to the results of the DSC thermal analysis.

Table 4. Summarization of the DSC results from the paraffin wax sample.

Sample	T_m [°C]	T_s [°C]	ΔH_m [kJ/kg]
Paraffin wax	48	52	202

3.2. Melting Performance of the PCM Unit

　　Relying on the experimental setup and procedure described above, trials of case studies were carried out to analyze the melting performance of the PCM unit. Figure 5 shows the transient temperature variation in each measuring point in the PCM unit during the initial charging period of 30 min. The initial PCM temperature was maintained at 25 °C, while the inlet HTF temperature and flow rate were kept constant at 68 °C and 7 L/min, respectively. During the initial charging period, the temperature difference between the

inlet and outlet HTF was observed due to the inlet HTF temperature being much higher than the PCM temperature, resulting in the heat transfer from the HTF to the PCM. The PCM temperature between the fins (T_{103}) rose dramatically in the initial period, which was caused by the large temperature difference between the HTF and the PCM. As T_{103} approached its melting temperature, its temperature rising rate gradually slowed down for a while. This was because the solid–liquid phase change of the paraffin wax absorbed the thermal energy of the HTF by using its latent heat. After the solid–liquid phase change of the paraffin wax was finished, T_{103} continued to rise slowly as the temperature difference between the HTF and the PCM shrunk. It was observed that both T_{102} and T_{104} were higher than T_{103} for the whole charging process, which meant the temperature gradient between the rectangular fins and the PCM existed. Comparing T_{105} and T_{103}, the time for the PCM between fins to melt was much shorter than for that without fins. The reason was that the fins employed expanded the heat transfer area significantly between the HTF and the PCM, which enhanced the charging rate greatly. Moreover, the PCM temperature was always lower than the HTF temperature during the entire charging process, which can be illustrated as follows. Firstly, the heat transfer rate between the HTF and the PCM decreased with the reduction in natural convection in the PCM unit when all the PCM was melted completely. Secondly, the thermal loss from the shell of the PCM unit to the ambient environment without insulation prevented the PCM temperature from increasing inevitably.
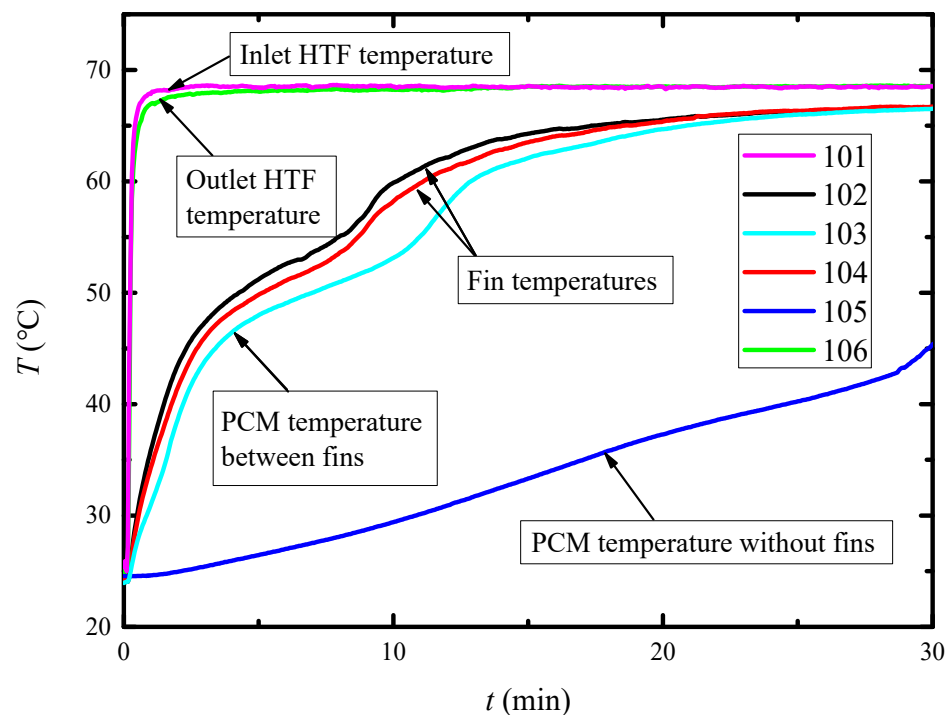

Figure 5. Transient temperature variation in each measuring point in the PCM unit during its charging period.

Photographs of the PCM unit were used to profoundly analyze the melting performance of the PCM during the charging process. Figure 6 shows the melting procedure of the paraffin wax during different stages of the charging process when T_{HTF} = 68 °C and q_{HTF} = 7 L/min. At the beginning of the melting procedure (Figure 6a), the solid paraffin wax began to expand upward owing to the heat transfer between the HTF and the PCM and the density difference between the solid state and the liquid state of the paraffin wax, indicating that thermal conduction was the present dominant driving force of the melting procedure. As time elapsed (Figure 6b), natural convection took place in the liquid paraffin wax due to the increase in the liquid fraction of the paraffin wax. At this moment, the buoyancy force of the liquid paraffin wax grew strong enough to overcome the flow

resistance caused by the viscous force. It was observed that the paraffin wax was firstly heated up and turned to the liquid state in the upper layer. Then, the liquid paraffin wax contacted with the solid paraffin wax along with the solid–liquid interface with the help of natural convection, which accelerated the melting rate further. As the liquid fraction of the paraffin wax in the PCM unit further increased (Figure 6c), the solid–liquid interface gradually moved to the lower layer, and liquid paraffin wax from the lower layer came up to the upper layer, which improved the melting rate significantly. From Figure 6d, most of the paraffin wax was melted in the PCM unit, except for some around the wall corner in the lower layer of the unit. The main reason was that the thermal loss from the shell of the PCM unit to the ambient environment slowed down the melting rate. No difference could be observed from Figure 6e,f, as the paraffin wax had fully melted at that moment.
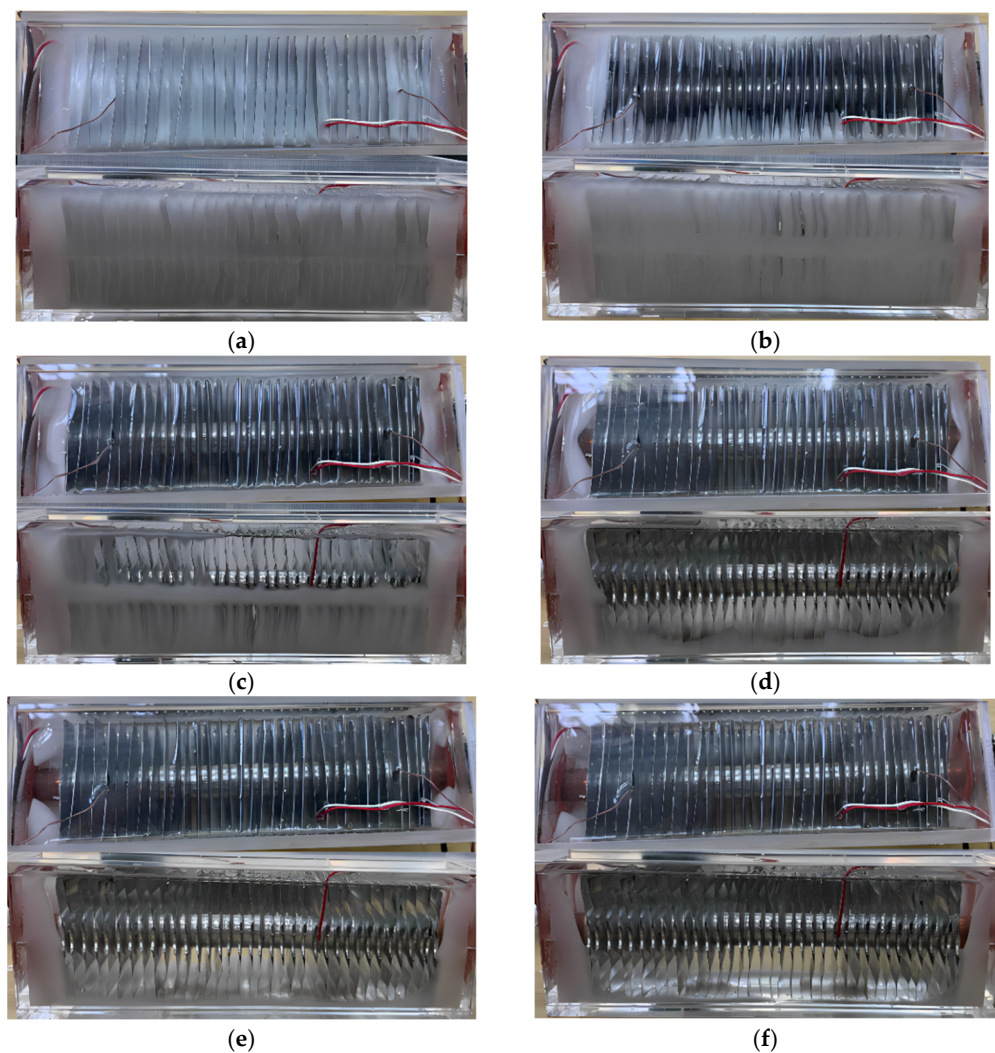

(a)

(b)

(c)

(d)

(e)

(f)

Figure 6. Melting procedure of paraffin wax during different stages of the charging process when $T_{\text{HTF}} = 68\ °C$ and $q_{\text{HTF}} = 7\ \text{L/min}$. (**a**) 5 min; (**b**) 10 min; (**c**) 15 min; (**d**) 20 min; (**e**) 25 min; (**f**) 30 min.

The total charging time was defined as the time when T_{103} reached a relatively steady temperature during the melting procedure, which was also the time when the temperature changing rate of T_{103} was approaching zero and had a tendency to rise at the same time. For that purpose, the temperature changing rate of T_{103} when $T_{\text{HTF}} = 68\ °C$ and $q_{\text{HTF}} = 7\ \text{L/min}$ was calculated and is described in Figure 7. Two thermal energy storage stages can be found in Figure 7: the phase change thermal energy storage stage (Stage 1) and the sensible thermal energy storage stage (Stage 2). In addition, the total charging time was considered to be the dividing line of these two stages. The total absorbed thermal energy storage and

average charging rate were calculated using Equations (1) and (2), respectively. Table 5 shows the thermal energy storage characteristics of the PCM thermal energy storage unit when $T_{HTF} = 68\,^{\circ}C$ and $q_{HTF} = 7\,L/min$. It is worth noting that the charging time determined based on the measuring thermocouple of T_{103} was relatively shorter than that obtained from the melting photographs in Figure 6, which was possibly owing to the temperature non-uniformity of the paraffin wax during the charging process.
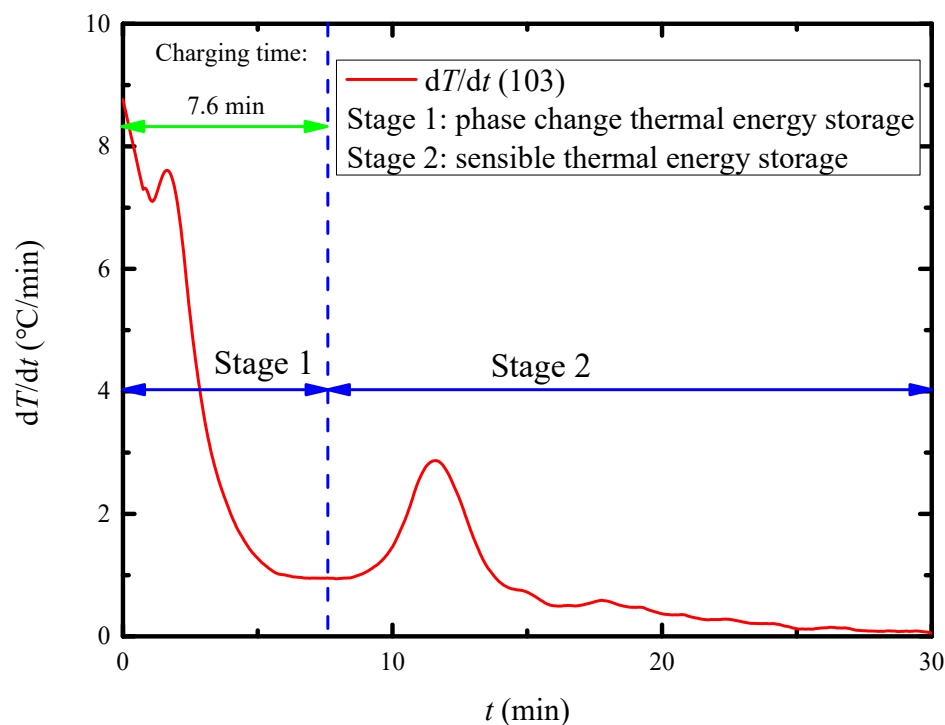

Figure 7. Temperature changing rate of T_{103} when $T_{HTF} = 68\,^{\circ}C$ and $q_{HTF} = 7\,L/min$.

Table 5. Thermal energy storage characteristics when $T_{HTF} = 68\,^{\circ}C$ and $q_{HTF} = 7\,L/min$.

Parameter	Value	Unit
P_{ch}	241.69	[W]
Q_{ch}	110.21	[kJ]
t_{ch}	7.6	[min]

4. Discussion

4.1. Influence of Inlet HTF Temperature

Several case studies were performed to analyze the influence of the inlet HTF temperature on the melting performance of the PCM unit. Two different inlet HTF temperatures were selected as 57 and 68 $^{\circ}C$, respectively, for this experimental research, and the HTF flow rate and initial paraffin wax temperature in the case studies were maintained at 7 L/min and 25 $^{\circ}C$, respectively.

Figure 8 compares the melting performance of the paraffin wax during different stages of the charging procedure with inlet HTF temperatures of 57 and 68 $^{\circ}C$, respectively. The liquid fraction of the paraffin wax in the PCM unit with a higher inlet HTF temperature was always higher than that with a lower inlet HTF temperature at the same time. It was speculated that a higher inlet HTF temperature led to less charging time and a faster charging rate from the HTF to the PCM. The main reason was that an improvement in the inlet HTF temperature resulted in a higher temperature gradient near the finned-tube surface. However, it diminished as time elapsed.
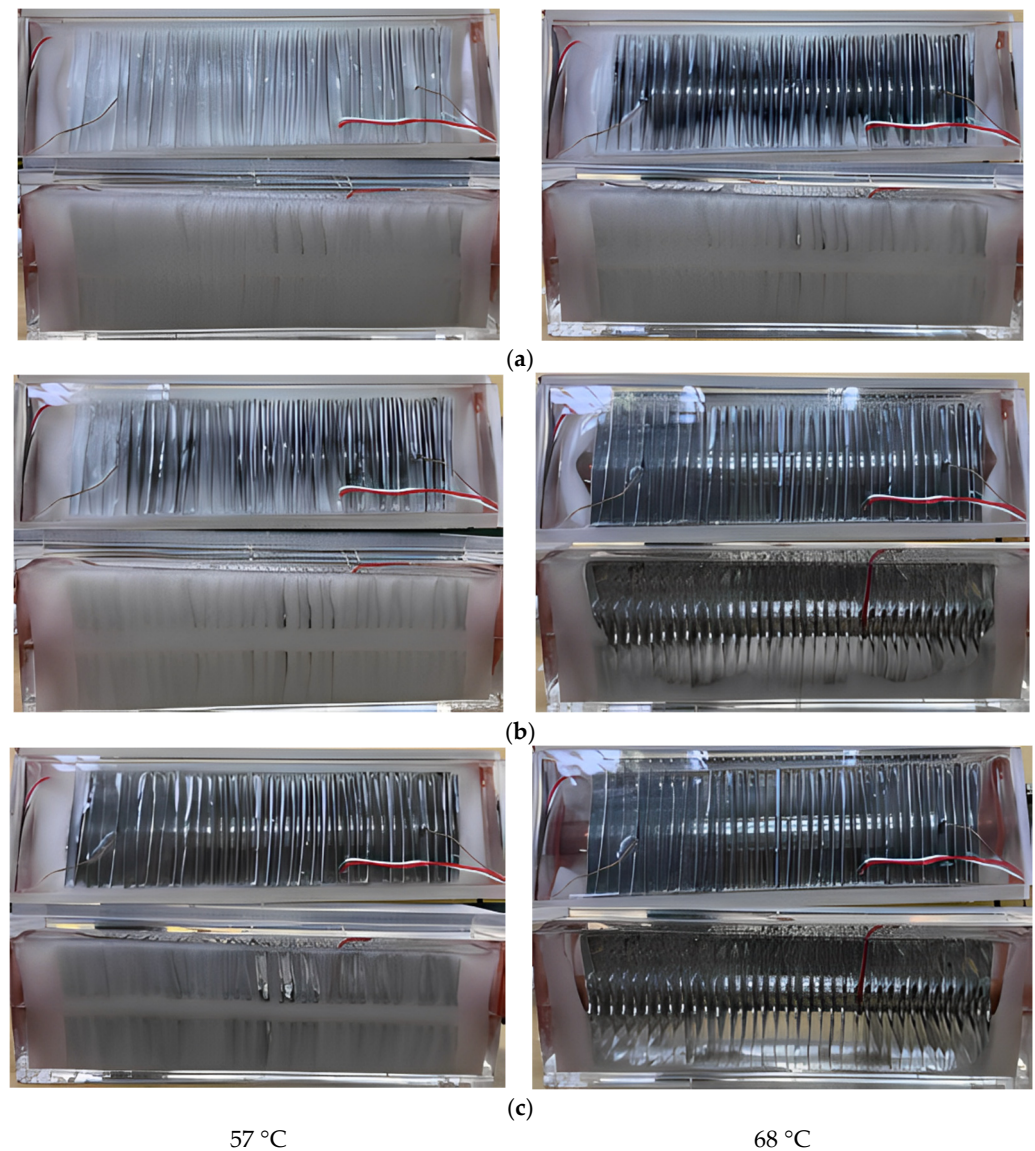
(a)

(b)

(c)

57 °C	68 °C

Figure 8. Melting performance of paraffin wax during different stages of the charging procedure with inlet HTF temperatures of 57 and 68 °C. (**a**) 10 min; (**b**) 20 min; (**c**) 30 min.

Table 6 summarizes the characteristics of the PCM unit with inlet HTF temperatures of 57 and 68 °C, respectively. The compared results indicated that the total charging time and average charging rate were significantly influenced by the inlet HTF temperature. The total charging time was reduced by 62.38% and the average charging rate was increased by 165.51% when the inlet HTF temperature was increased from 57 to 68 °C. The reason was that the melting rate between the HTF and the PCM was enhanced when the temperature difference between them became large, which caused the much shorter total charging time required for the PCM unit. Since the given mass of paraffin wax was constant, the total heat storages with inlet HTF temperatures of 57 and 68 °C during the charging procedure were nearly equivalent.

4.2. Influence of HTF Flow Rate

The influence of the HTF flow rate on the melting performance of the PCM unit was analyzed by maintaining the inlet HTF temperature and initial paraffin wax temperature at 68 °C and 25 °C, respectively. Three HTF flow rates were selected in the experiments, which were 4, 7 and 10 L/min, respectively.

Table 6. Characteristics with inlet HTF temperatures of 57 and 68 °C.

Parameter	Value		Unit
	T_{HTF} = 57 °C	T_{HTF} = 68 °C	
P_{ch}	91.03	241.69	[W]
Q_{ch}	110.33	110.21	[kJ]
t_{ch}	20.2	7.6	[min]

Figure 9 compares the melting performance of the paraffin wax during different stages of the charging procedure with HTF flow rates of 4, 7 and 10 L/min, respectively. As seen from the figure, the influence of the HTF flow rate on the melting performance of the paraffin wax was negligible. Evidence could also be found in Figure 10, which depicts the comparison of T_{103} in the PCM unit with HTF flow rates of 4, 7 and 10 L/min. No significant changes in T_{103} were examined during the charging procedure with HTF flow rates of 4, 7 and 10 L/min. Considering that a higher HTF flow rate requires more pumping power, a lower value of HTF flow rate was suggested for an energy efficient LTES unit.
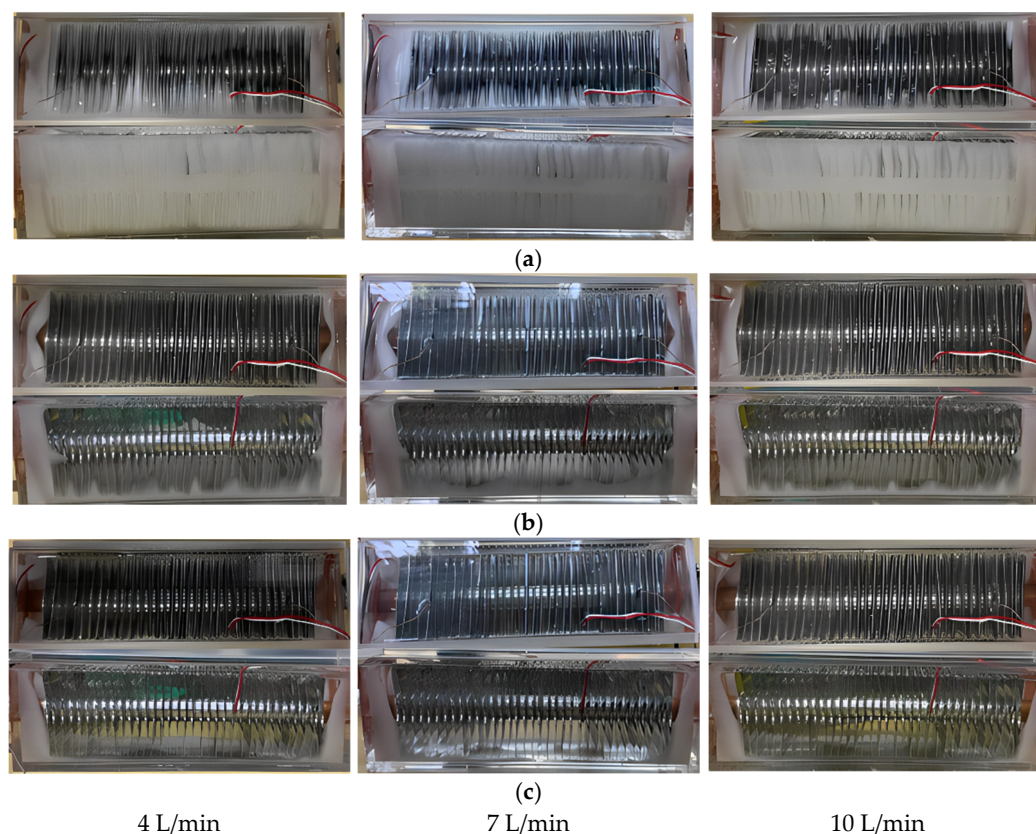

(a)

(b)

(c)

4 L/min　　　　　　　　　7 L/min　　　　　　　　　10 L/min

Figure 9. Melting performance of paraffin wax during different stages of the charging procedure with HTF flow rates of 4, 7 and 10 L/min. (**a**) 10 min; (**b**) 20 min; (**c**) 30 min.

Table 7 summarizes the characteristics of the PCM unit with HTF flow rates of 4, 7 and 10 L/min, respectively. The total charging time was only reduced by 2.63% and the average charging rate was just increased by 0.53% when the HTF flow rate was increased from 7 to 10 L/min, which showed no obvious influence of the HTF flow rate during the charging procedure of the PCM unit. This can be explained as follows. During the charging procedure, the thermal heat of the HTF was firstly transferred to the finned tube, and then the finned tube released this thermal heat to the paraffin wax. Meanwhile, the heat transfer coefficient between the HTF and the finned tube was greater than that between the finned tube and the paraffin wax in magnitude, which dominated the total melting rate of the PCM

unit. As a result, a faster HTF flow rate was able to improve the heat transfer coefficient between the finned tube and the paraffin wax to a certain degree, but barely improved the total melting rate of the PCM unit.
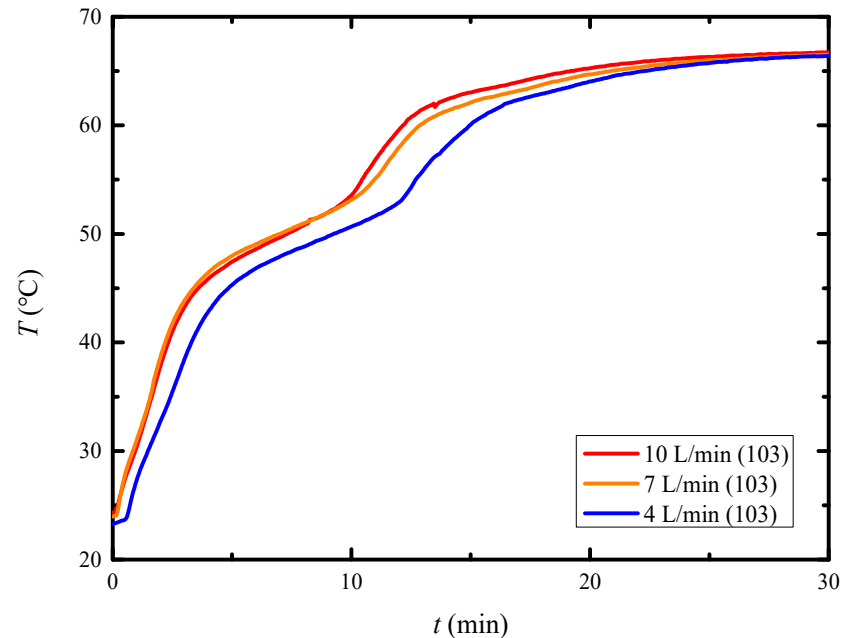

Figure 10. Comparison of T_{103} values with HTF flow rates of 4, 7 and 10 L/min.

Table 7. Characteristics with HTF flow rates of 4, 7 and 10 L/min.

Parameter	Value			Unit
	q_{HTF} = 4 L/min	q_{HTF} = 7 L/min	q_{HTF} = 10 L/min	
P_{ch}	194.47	241.69	242.98	[W]
Q_{ch}	110.85	110.21	107.88	[kJ]
t_{ch}	9.5	7.6	7.4	[min]

5. Conclusions

A case study was carried out to analyze the charging process and evaluate the influence of the inlet HTF temperature and the flow rate on the melting performance of paraffin wax. A shell-and-tube unit with a novel rectangular fin configuration was designed and manufactured for visualized melting photographs. Conclusions were drawn as follows:

(1)   The PCM unit with rectangular fins showed the potential for enhancing the melting performance when compared to that without fins. By visualization, the performance was dominated by thermal conduction in the initial state. As time elapsed, natural convection developed to accelerate the melting rate of the PCM.

(2)   The inlet HTF temperature had a great influence on the characteristics compared with the inlet HTF flow rate. The total charging time was reduced by 62.38% and the average charging rate was increased by 165.51% when the inlet HTF temperature was increased from 57 to 68 °C.

(3)   The higher value of the inlet HTF temperature and the lower value of the HTF flow rate were suggested to improve the energy storage efficiency and reduce the energy consumption of the LTES unit at the same time.

With the potentially wide use of TES technology in the near future, the development of the shell-and-tube unit with a novel rectangular fin configuration could provide helpful guides and insights when designing the TES system and choosing appropriate working conditions for improved working efficiency. Considering the shell-and-tube structure with

only one tube in this study was a basic unit of a multi-tubular heat exchanger, we also plan to apply this rectangular fin configuration to the multi-tubular heat exchanger device in heat pump systems for space heating from now on.

Nomenclature

Abbreviation

DSC	differential scanning calorimeter
HTF	heat transfer fluid
LTES	latent thermal energy storage
PCM	phase change material
TES	thermal energy storage

Symbols

cp	specific heat capacity ($J \cdot kg^{-1} \cdot K^{-1}$)
Δf	uncertainty of experiment
ΔH_m	latent heat of fusion ($J \cdot kg^{-1}$)
l	location of thermocouples (m)
m	mass (kg)
n	number of intervals
P_{ch}	average charging rate (W)
Q_{ch}	total heat storage (J)
q	mass flow rate ($kg \cdot s^{-1}$)
T	temperature (°C)
t_{ch}	total charging time (s)

Subscript

ch	charging
HTF	heat transfer fluid
in	inlet
m	melting
out	outlet
PCM	phase change material
s	solidification
101	thermocouple 101
102	thermocouple 102
103	thermocouple 103
104	thermocouple 104
105	thermocouple 105
106	thermocouple 106

References

1. Dowd, A.-M.; Hobman, E. Mobilizing citizens for a low and clean energy future. *Curr. Opin. Environ. Sustain.* **2013**, *5*, 191–196. [CrossRef]
2. Jiang, L.; Roskilly, A.; Wang, R.; Wang, L.; Lu, Y. Analysis on innovative modular sorption and resorption thermal cell for cold and heat cogeneration. *Appl. Energy* **2017**, *204*, 767–779. [CrossRef]
3. Jiang, L.; Wang, R.; Wang, L.; Roskilly, A. Investigation on an innovative resorption system for seasonal thermal energy storage. *Energy Convers. Manag.* **2017**, *149*, 129–139. [CrossRef]

4. Said, M.; Hassan, H. Parametric study on the effect of using cold thermal storage energy of phase change material on the performance of air-conditioning unit. *Appl. Energy* **2018**, *230*, 1380–1402. [CrossRef]

5. Gude, V.G. Energy storage for desalination processes powered by renewable energy and waste heat sources. *Appl. Energy* **2015**, *137*, 877–898. [CrossRef]

6. Wang, Z.; Zhang, H.; Xia, X. Experimental investigation on the thermal behavior of cylindrical battery with composite paraffin and fin structure. *Int. J. Heat Mass Transf.* **2017**, *109*, 958–970. [CrossRef]

7. Karthick, K.; Suresh, S.; Joy, G.C.; Dhanuskodi, R. Experimental investigation of solar reversible power generation in Thermoelectric Generator (TEG) using thermal energy storage. *Energy Sustain. Dev.* **2018**, *48*, 107–114. [CrossRef]

8. Jiang, L.; Lu, Y.; Tang, K.; Wang, Y.; Wang, R.; Roskilly, A.; Wang, L. Investigation on heat and mass transfer performance of novel composite strontium chloride for sorption reactors. *Appl. Therm. Eng.* **2017**, *121*, 410–418. [CrossRef]

9. Raul, A.K.; Bhavsar, P.; Saha, S.K. Experimental study on discharging performance of vertical multitube shell and tube latent heat thermal energy storage. *J. Energy Storage* **2018**, *20*, 279–288. [CrossRef]

10. Seddegh, S.; Wang, X.; Joybari, M.M.; Haghighat, F. Investigation of the effect of geometric and operating parameters on thermal behavior of vertical shell-and-tube latent heat energy storage systems. *Energy* **2017**, *137*, 69–82. [CrossRef]

11. Fornarelli, F.; Ceglie, V.; Fortunato, B.; Camporeale, S.; Torresi, M.; Oresta, P.; Miliozzi, A. Numerical simulation of a complete charging-discharging phase of a shell and tube thermal energy storage with phase change material. *Energy Procedia* **2017**, *126*, 501–508. [CrossRef]

12. Kibria, M.; Anisur, M.; Mahfuz, M.; Saidur, R.; Metselaar, I. Numerical and experimental investigation of heat transfer in a shell and tube thermal energy storage system. *Int. Commun. Heat Mass Transf.* **2014**, *53*, 71–78. [CrossRef]

13. Seddegh, S.; Joybari, M.M.; Wang, X.; Haghighat, F. Experimental and numerical characterization of natural convection in a vertical shell-and-tube latent thermal energy storage system. *Sustain. Cities Soc.* **2017**, *35*, 13–24. [CrossRef]

14. Akgün, M.; Aydın, O.; Kaygusuz, K. Experimental study on melting/solidification characteristics of a paraffin as PCM. *Energy Convers. Manag.* **2007**, *48*, 669–678. [CrossRef]

15. Medrano, M.; Yilmaz, M.; Nogués, M.; Martorell, I.; Roca, J.; Cabeza, L.F. Experimental evaluation of commercial heat exchangers for use as PCM thermal storage systems. *Appl. Energy* **2009**, *86*, 2047–2055. [CrossRef]

16. Macphee, D.W.; Erguvan, M. Thermodynamic Analysis of a High-Temperature Latent Heat Thermal Energy Storage System. *Energies* **2020**, *13*, 6634. [CrossRef]

17. Yang, X.; Lu, Z.; Bai, Q.; Zhang, Q.; Jin, L.; Yan, J. Thermal performance of a shell-and-tube latent heat thermal energy storage unit: Role of annular fins. *Appl. Energy* **2017**, *202*, 558–570. [CrossRef]

18. Yang, X.; Yu, J.; Guo, Z.; Jin, L.; He, Y.-L. Role of porous metal foam on the heat transfer enhancement for a thermal energy storage tube. *Appl. Energy* **2019**, *239*, 142–156. [CrossRef]

19. Amini, A.; Miller, J.; Jouhara, H. An investigation into the use of the heat pipe technology in thermal energy storage heat exchangers. *Energy* **2017**, *136*, 163–172. [CrossRef]

20. Vivekananthan, M.; Amirtham, V.A. Characterisation and thermophysical properties of graphene nanoparticles dispersed erythritol PCM for medium temperature thermal energy storage applications. *Thermochim. Acta* **2019**, *676*, 94–103. [CrossRef]

21. Pathak, S.; Jain, K.; Kumar, P.; Wang, X.; Pant, R. Improved thermal performance of annular fin-shell tube storage system using magnetic fluid. *Appl. Energy* **2019**, *239*, 1524–1535. [CrossRef]

22. Abdulateef, A.M.; Mat, S.; Abdulateef, J.; Sopian, K.; Al-Abidi, A.A. Geometric and design parameters of fins employed for enhancing thermal energy storage systems: A review. *Renew. Sustain. Energy Rev.* **2018**, *82*, 1620–1635. [CrossRef]

23. Aly, K.A.; El-Lathy, A.R.; Fouad, M.A. Enhancement of solidification rate of latent heat thermal energy storage using corrugated fins. *J. Energy Storage* **2019**, *24*, 100785. [CrossRef]

24. Deng, S.; Nie, C.; Jiang, H.; Ye, W.-B. Evaluation and optimization of thermal performance for a finned double tube latent heat thermal energy storage. *Int. J. Heat Mass Transf.* **2018**, *130*, 532–544. [CrossRef]

25. Vogel, J.; Johnson, M. Natural convection during melting in vertical finned tube latent thermal energy storage systems. *Appl. Energy* **2019**, *246*, 38–52. [CrossRef]

26. Deng, S.; Nie, C.; Wei, G.; Ye, W.-B. Improving the melting performance of a horizontal shell-tube latent-heat thermal energy storage unit using local enhanced finned tube. *Energy Build.* **2018**, *183*, 161–173. [CrossRef]

27. Bhagat, K.; Prabhakar, M.; Saha, S.K. Estimation of thermal performance and design optimization of finned multitube latent heat thermal energy storage. *J. Energy Storage* **2018**, *19*, 135–144. [CrossRef]

28. Lin, Y.; Jia, Y.; Alva, G.; Fang, G. Review on thermal conductivity enhancement, thermal properties and applications of phase change materials in thermal energy storage. *Renew. Sustain. Energy Rev.* **2018**, *82*, 2730–2742. [CrossRef]

29. Yu, M.; Zhang, C.; Fan, Y.; Zhang, X.; Zhao, Y. Performance study of phase change charging/discharging processes of condensing heat storage in cold regions based on a mathematical model. *Appl. Therm. Eng.* **2020**, *182*, 115805. [CrossRef]

30. Moffat, R.J. Describing the uncertainties in experimental results. *Exp. Therm. Fluid Sci.* **1988**, *1*, 3–17. [CrossRef]